Metrol. Meas. Syst., Vol. 30 (2023) No. 1, pp. 3–16
DOI: 10.24425/mms.2023.144397

PAN POLSKA AKADEMIA NAUK

METROLOGY AND MEASUREMENT SYSTEMS
Index 330930, ISSN 0860-8229
www.metrology.wat.edu.pl

M&MS

ESTABLISHING AND CHARACTERIZING A PERMANENT MAGNET SYSTEM FOR THE PROTOTYPE OF NIS'S KIBBLE BALANCE

Sayed Emira[1)], E.R. Shaaban[2)], M.M. Rashad[3)], Shaker A. Gelany[1)]

1) National Institute of Standards (NIS), Tersa St, El-Haram, PO Box 136, Code 12211, Giza, Egypt
(✉ *ph_sayed2014@yahoo.com, shaker9595@yahoo.com*)
2) Department of Physics, Faculty of Science, Al-Azhar University, Assiut 71542, Egypt
(*esam_ramadan2008@yahoo.com*)
3) Central Metallurgical Research and Development Institute (CMRDI), P.O. BOX.87 Helwan, Egypt11421
(*rashad133@yahoo.com*)

Abstract

The Kibble balance experiment is used to redefine the kilogram as a unit of mass based on the Planck constant. To demonstrate and understand the basic principle of the Kibble balance, the National Institute of Standards (NIS)-Egypt has constructed a prototype Kibble balance that can measure gram-level masses with 0.01% relative uncertainty. Through the construction of this prototype, the challenges can be studied and addressed to overcome the weaknesses of NIS's prototype. This study presents the design and construction of the prototype Kibble balance. It also focuses on the design and performance of the magnetic system, which is a crucial element of the Kibble balance. Analytical modeling and finite element analysis were used to evaluate and improve the magnet system. Several other aspects were also discussed, including the yoke's material and enhancing the magnetic profile within the air gap of the magnet system. Over a vertical distance of 30 mm inside the air gap, the magnetic flux density was found to be 0.3 T, and the uniformity was found to be 8×10^{-5}.

Keywords: Kibble balance, Planck constant, magnet system, magnetic field.

1. Introduction

In 2019, the International System of Units (SI-Units) was amended to relate the basic SI units to natural physical constants [1,2]. In the restructuring, the kilogram, the SI mass unit, was revised in respect of the Planck constant [3,4]. There are currently two experimental techniques that can establish the relationship between mass (m) and the Planck constant ($\hbar$) with 10 parts per billion relative uncertainties [5, 6]. The first technique is *X-ray crystal density* (XRCD) which counts atoms in a 1 kg silicon sphere [7]. The second technique is the watt balance, also known as the Kibble Balance (KB) [8]. The KB is a highly complicated and sophisticated measuring instrument.

Article history: received August 13, 2022; revised November 6, 2022; accepted November 20, 2022; available online January 23, 2023.

Establishing such a system requires significant financial and infrastructural investments, as well as a higher level of scientific and technological knowledge [9]. Many *National Metrology Institutes* (NMIs) are unable to construct this facility due to a lack of necessary knowledge and resources. This has restricted the NMIs' ability to carry out KB construction in their own countries. The metrology institutes need the KBs to provide traceable measurements of mass standards with an acceptable level of uncertainty. One of the options to meet this need with minimum financial and technological knowledge is to establish a KB suitable for masses well below 1 kg. This level of mass measurement does not require the establishment of a permanent magnetic system with a large volume. Moreover, it is simpler to operate and easier to maintain. The *National Institute of Standards* (NIS-Egypt) is one of several NMIs considering this opportunity. The National Institute of Standards (NIS)-Egypt has constructed a prototype Kibble balance that can measure gram-level masses (10-gram) with 0.01% relative uncertainty. Furthermore, the study aims to improve this value to correspond with the uncertainty achievable via a subdivision method for calibrating standard weights of accuracy class F_2 according to OIML R111 [10].

Through the construction of this prototype, the challenges can be studied and addressed to overcome the weaknesses of NIS's prototype. This study presents the design and construction of the prototype Kibble balance. It also focuses on the design and performance of the magnetic system, which is a crucial element of the Kibble balance. Analytical modelling and finite element analysis were used to evaluate and improve the magnet system. Several other aspects were also discussed, including the yoke's material and enhancing the magnetic profile within the air gap of the magnet system.

2. Fundamentals of Kibble balance

The KB is an electromechanical system that compares electrical and mechanical power. A KB's operational phases comprise force and dynamic (or velocity). In the force stage (static stage), the gravitational force ($m.g$) acting on a mass (m) is compared to the force of electromagnetic power as a result of passing an electric current (I) through a coil of length (L) immersed in a magnetic field (B). The following equation (1) describes this equilibrium (Lorentz force):

$$mg = (BL)_{\text{static}} I. \tag{1}$$

In the dynamic stage, the KB overcomes the challenges of measuring magnetic field (B) and coil length (L). A voltage difference (U) is produced across the ends of the coil when the same coil moves through the same magnetic field at a specified velocity, v (Faraday's law):

$$U = (BL)_{\text{dynamic}} v. \tag{2}$$

The magnetic field and the length of the coil were the same during both phases, and the coil maintains the same alignment as it moves through its weighing stage while it is in its dynamic stage. Equations (1) and (2) may be simplified by eliminating the geometrical factor, BL:

$$mgv = UI. \tag{3}$$

Because it compares mechanical and electrical power, it was known as the "watt balance". Using this property, the Kibble balance experiment relates electrical power to the Planck constant. The following form may be used to express electrical power (W_e):

$$W_e = UI. \tag{4}$$

Metrol. Meas. Syst., Vol. 30 (2023), No. 1, pp. 3–16
DOI: 10.24425/mms.2023.144397

Ohm's law states that current I is expressed as $I = V/R$, where V is the voltage drop across a standard reference resistor R:

$$W_e = U \cdot V/R. \tag{5}$$

Using the quantized Hall resistance, the resistance value R_{90} may be calculated, and using the conventional constants, R_{K-90} and K_{J-90}, the voltages may be measured related to the Josephson voltage standard [11, 12]. Consequently, the electrical power may be described as:

$$W_e = \frac{U_{90} \cdot V_{90}}{R_{90}} \cdot \frac{K_{J-90}^2 \cdot R_{K-90}}{4} h, \tag{6}$$

where:

$$\begin{aligned} R &= R_{90} \frac{R_K}{R_{K-90}} \quad \text{with} \quad R_K = \frac{h}{e^2}, \\ U &= U_{90} \frac{K_{J-90}}{K_J} \quad \text{with} \quad K_J = \frac{2e}{h}. \end{aligned} \tag{7}$$

While the mechanical power depends on the mass m as well as other quantities like velocity v and acceleration due to gravity g, the mechanical power equation may be written as follows:

$$W_m = mgv. \tag{8}$$

An electrical power in equation (6) is compared to the mechanical power in equation (8) using a Kibble balance, which leads to the following equation:

$$mgv = UI = \frac{U_{90} \cdot V_{90}}{R_{90}} \cdot \frac{K_{J-90}^2 \cdot R_{K-90}}{4} h, \tag{9}$$

where U_{90} is the conventional voltage measured in the dynamic mode, V_{90} is the conventional voltage measured in the static mode, and R_{90} is the conventional resistance value of the resistor used in the static mode. For the local gravity acceleration measurement, this higher accuracy can be achieved using an absolute gravimeter traceable to a primary standard of time and length. An interferometry system, *i.e.* a heterodyne Michelson interferometer, could be used to measure vertical velocity. However, since this is a prototype for calibrating masses at the level of a gram, such high-precision measurement equipment was not necessary for a basic experimental setup like the one utilized in this study.

3. Mechanical structure and facilities

The moving mechanisms of a Kibble balance can be divided based on the type of the center pivot into two groups. One is knife edge-based with a balance beam or a wheel as described by *e.g.*, the *National Institute of Standards and Technology* (NIST) [9]. The other is flexure-pivot-based balance as approved by *e.g.*, *Bureau International des Poids et Mesures* (BIPM) [6]. The prototype KB was designed to measure mass at gram-level masses by modifying one of the NIS mass lab's oldest two-pan equal-arm balances. Figure 1a shows a two-pan equal-arm balance before modification (manufactured by A. Ruprecht Wien with a capacity of 1 kg). Figure 1b shows the equal-arm balance beam after modifications. For hanging the two pans, the two-pan equal-arm balance has a special crossed-knife edge suspension system. Three gimbals make up this suspension system. The first gimbal comprises a terminal bearing plane and a knife edge.

This knife edge and the terminal knife edge are parallel. To avoid tilting, the second suspension gimbal includes a bearing plane and a knife edge at a right angle to the first knife edge. A conical pivot is located at the lower end of the third gimbal to hang the pan. This mechanism can keep the vertical motion in the coil. Figure 1c illustrates the 3D CAD model of NIS's KB.

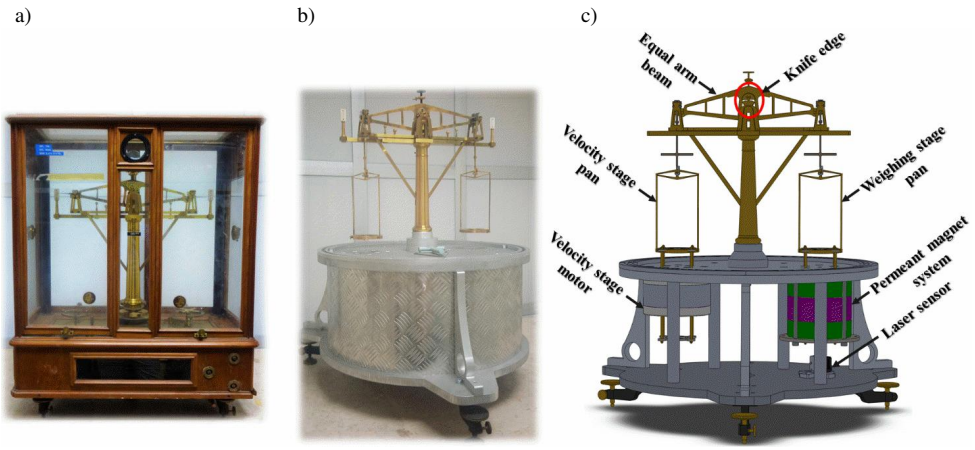

Fig. 1. The KB illustration: a) Two-pan equal-arm balance before modification, b) Modified KB and c) 3D CAD model of NIS's KB.

Figure 2 illustrates the schematic layout of the setup. The permanent magnet system with coil suspension will be discussed in Section 4 of this article. In the force stage, the measuring coil is connected to a controllable current source (Model 121, Lake Shore) to provide current to the coil. The measuring system comprises a standard reference resistor of 100 ohms (Model CER6000, WIKA) with a temperature coefficient of less than one ppm per °C, and a reference multimeter with a GPIB interface bus (Model 8508A, Fluke) is used to measure the current supplied to the coil. These instruments have been calibrated by the Electrical Quantity Metrology Laboratory

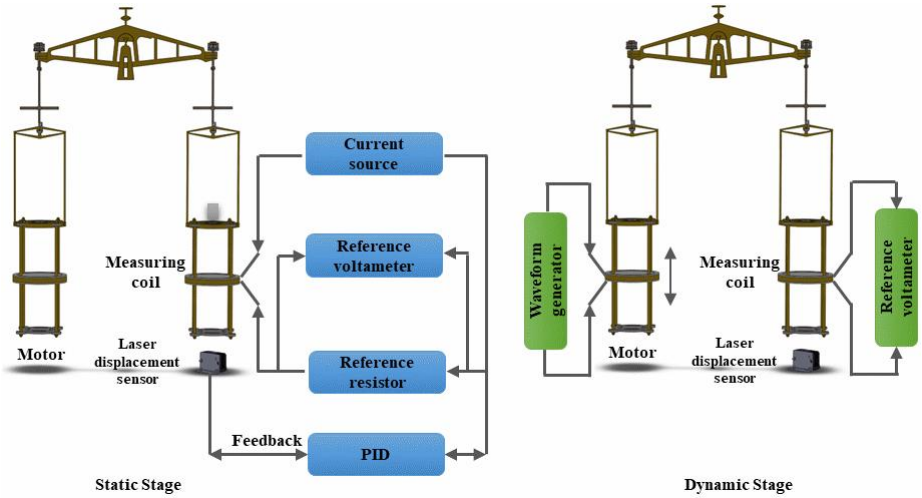

Fig. 2. Schematic layout of the setup.

Metrol. Meas. Syst., Vol. 30 (2023), No. 1, pp. 3–16
DOI: 10.24425/mms.2023.144397

(NIS), which is recognized internationally by the BIPM. To accurately detect the equilibrium state in the force stage, a laser displacement sensor (Model BD-30, Autonics) was utilized to optically track the movement of the measuring coil. This sensor has been calibrated by the Primary Length Standard and Laser Technology Laboratory, NIS. The lab maintains the primary length standard of Egypt, which is an iodine-stabilized He–Ne laser at 633 nm with a relative standard uncertainty of 2.5×10^{-11}. A programmable waveform generator (Model DG1022Z, RIGOL) is used with the motor in the dynamic stage to move the coil sinusoidally in the magnetic field. Using the computer and the LabView platform, the multifunction DAQ (T7, LabJak) creates and controls output-input signals for the balance.

4. Permanent magnet system

The rare-earth permanent magnet as a magnetic field source is mainly employed in watt balance experiments [8, 13]. The permanent magnet produces a magnetic field that affects the measuring coil causing a voltage drop when the coil travels vertically during the moving stage and a force when the coil is activated by current during the weighing stage. The experiment assumes that the magnetic flux density received by the coil stays constant between the two measurement stages, which can be efficiently achieved by a permanent magnet. Several NMIs, including BIPM, NIST, the *Federal Institute of Metrology* (METAS), and the *Korea Research Institute of Standards and Science* (KRISS), utilized a closed symmetrical structural magnet system with a yoke [14–17]. The closed symmetrical structural magnet system's main advantage is that it can produce an intense magnetic flux around the coil and a flat magnetic field in the air gap's center [18].

4.1. Description of the permanent magnet system

The proposed cylindrical magnet system is shown in Fig. 3.

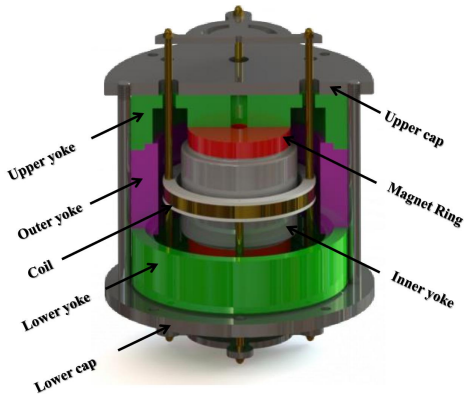

Fig. 3. Structure of the NIS permanent magnet assembly.

The magnetic field generated by a pair of ring-shaped permanent magnets opposite each other is directed by yokes manufactured from low-carbon steel. The magnetic material of the permanent magnet ring was made from Neodymium-Iron-Boron (NdFeB, N48 grade) with a remanence, B_r and relative permeability, of 1.4 T and 1.05 respectively. For the reasons outlined in the following paragraphs, NdFeB magnets were used as the magnet material to generate the radial magnetic

field. NdFeB magnet material has a low cost and is widely available on the market in different shapes and grades. Furthermore, it has a high magnetic energy output, which causes a reduction in the magnetic system's size. The influence of temperature fluctuations on the magnetic material is a disadvantage of NdFeB magnets. The Curie temperature for neodymium magnets is low, about 310 °C. Therefore, it has a high-temperature coefficient in the range of -1×10^{-3} K^{-1}. In the case of change of magnet temperature by –1 mK, the magnetic flux density changes by 1×10^{-6} [8]. However, controlling the operating environment's temperature may lessen this impact. This value is acceptable because the target relative uncertainty in the proposed prototype is within a part in 10^{-4}. Moreover, the temperature change is often very slow compared to the data collection cycle. By selecting a different grade of the permanent magnet material, the impact of temperature may be reduced. NIS adopted the decision to employ an alloy of SmCo, a permanent magnet with a much lower temperature coefficient, for the next generation of KB systems.

The NIS magnet system is detailed as shown in Fig. 4, with a ring magnet having an inner radius r_{inr} of 6.35 mm, an outer radius r_{out} of 38.1 mm, a height W_m, of 12.60 mm, a width of air gap W_g, of 17 mm, a coil radius r_c, of 51.60 mm, a height of precision air gap of 30 mm, a distance from the center of the inner yoke to the center of the permanent magnet h_m, of 41.8 mm, a total height of 146 mm, and an outer diameter of 160 mm.

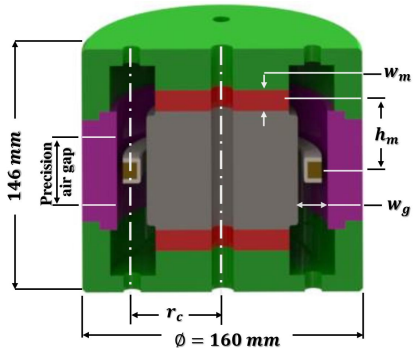

Fig. 4. Cross-section view of the NIS magnet system.

Figure 5 shows the suspension system of the measuring coil. The coil is wound using copper wire (AWG 34) with a diameter of 0.16 mm. The length of the wire determines BL for the measurement coil, with a minimal level of uncertainty reached when the BL value is between

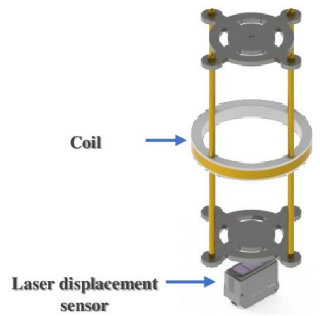

Fig. 5. Suspension system of the coil.

Metrol. Meas. Syst., Vol. 30 (2023), No. 1, pp. 3–16
DOI: 10.24425/mms.2023.144397

400 Tm and 1000 Tm [19]. The magnet system was given a value of 400 Tm. A coil former made of polytetrafluoroethylene (PTFE) was wound on with about 3980 turns in the center.

Moreover, to optimize the performance of the next-generation NIS Kibble balance, we have decided on the addition of lagging material and a custom-designed ring as one of the newest techniques utilized to protect copper wire against moisture absorption [20].

4.2. Designing the magnet system

The magnetic field profile is the functional relationship between the radial magnetic flux density and the air gap's vertical position. The magnetic flux must be homogeneous throughout the movement trajectory of the coil to maintain a constant induced voltage during coil movement with constant velocity [21,22]. The variation of magnetic flux modeling as well as the dependence of the magnetic profile and yoke permeability was carried out utilizing an analytical model and *finite element analysis* (FEA).

4.2.1. Analytical model analysis

The analytical model clearly shows the design concept of the permanent magnet and may be used as a guide to FEA software's extensive simulations. The magnetic flux density in the air gap B_g may be calculated using the following formula [23]:

$$B_g = \frac{B_r}{\dfrac{Dh_m}{\left(r_{\text{out}}^2 - r_{\text{inr}}^2\right)} + \mu_r \left(\dfrac{w_g}{w_m}\right)}, \tag{10}$$

where D is the coil diameter and the other equation parameters are discussed in detail in Section 4.1. The magnetic flux density within the air gap is calculated as 313 mT using the previously mentioned equation (10).

4.2.2. Finite element analysis

The FEA is used to design and simulate the magnetic circuit as well. A 3D geometrical model with the AC/DC module of the COMSOL Multiphysics software was used to run numerical simulations. Moreover, tetrahedral elements (mesh) were used, which are discussed in detail in Annex A. The governing equations of the AC/DC module are:

$$H = -\nabla V_m\,, \tag{11}$$

$$\nabla \cdot B = 0, \tag{12}$$

where H is the strength of the magnetic field, V_m is the scalar magnetic potential, and B is the magnetic flux density.

For the permanent magnet, the constitutive relationship is obtained from

$$B = \mu_0 \mu_{\text{rec}} H + B_r\,, \tag{13}$$

where μ_0 is vacuum permeability, μ_{rec} is the recoil permeability and B_r is the remnant magnetic flux density.

The distribution of magnetic flux inside the air gap is shown in Fig. 6. The profiles of the magnetic flux are displayed, ranging from red to blue in color density in two cross-sectional

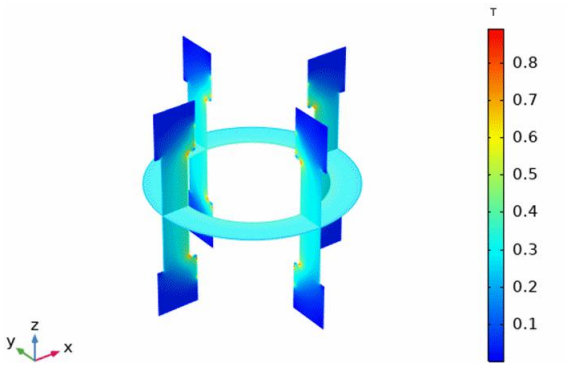

Fig. 6. Distribution of the magnetic flux in the air gap.

planes. The magnetic flux is focused at the inner edges due to the cylindrical shape, which is symmetric in both planes.

The blue line in Fig. 7 represents the results for magnetic flux density in a vertical position in a 50 mm air gap (±25 mm), whereas the red line represents the results for magnetic flux density in a precision air gap of 30 mm height (±15 mm).

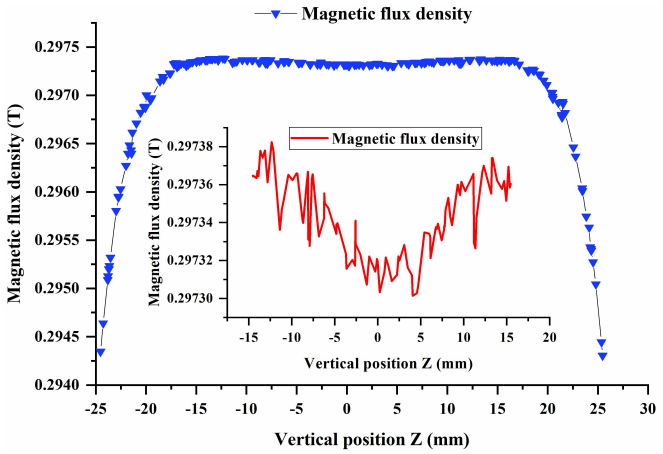

Fig. 7. Magnetic flux density variation.

The FEA results in a flux density value of about 297 mT, whereas the analytical model (Section 4.2.1, equation 10) produces a value of 313 mT. Therefore, there is a difference between the analytical model and the FEA with a relative difference of 5%. This difference is because of the analytical model equation (10), which indicates that the flux density value in the gap is produced in the absence of both saturation of the field in the yoke material and flux leakage. In a ±15 mm air gap height (precision air gap) around the symmetry axis, the relative change of the magnetic flux density remains within a range of 8×10^{-5}. However, the publications of Kibble balances report typical relative variations of the magnetic flux over the air gap's height to be about 10^{-4} [8, 24]. The BIPM and NIST reported a relative variation in magnetic field values of about 2×10^{-5} and 1×10^{-5}, respectively [18, 19].

Metrol. Meas. Syst., Vol. 30 (2023), No. 1, pp. 3–16
DOI: 10.24425/mms.2023.144397

4.3. Optimization of the permanent magnet system

The value of the magnetic field and its flatness profile within the air gap depend on several factors, such as the coil radius (r), the air gap width (W_g), and the relative permeability of the yoke material as per equation (10). Furthermore, in Kibble balance experiments, a flat field profile reduces uncertainties [15]. Therefore, this section focuses on studying and optimizing these parameters to improve the flatness of the field profile and the target uncertainty.

4.3.1. Magnetic flux versus coil radius

The radial magnetic flux density has two components, Br(z) and Br(r). Br(z) is the magnetic flux in the vertical direction discussed in the previous section, and Br(r) is the magnetic flux in the horizontal direction. It is significant to consider that the magnetic flux density within the air gap is proportional to $1/r$ while designing the magnet system (r is the coil radius) [25]. The advantage is that the systematic effect of thermal expansion on coil geometry is reduced. Moreover, the magnetic field will be less sensitive to coil misalignment [26]. The variation of the magnetic flux in the horizontal direction in the air gap is examined by employing the FEA. The magnetic flux was studied for seven sections in the range of –3 mm: w_0: +3 mm with a 1-millimeter step for the air gap width of 17 mm (w_0 is the center of the air gap). It can be shown in Fig. 8a that the magnetic flux density has an inverse relationship to the coil's radius, increasing with a decreasing coil radius and decreasing with an increasing coil radius. The center of the air gap has good flatness with a minimum relative deviation, as shown in Figure 8b.

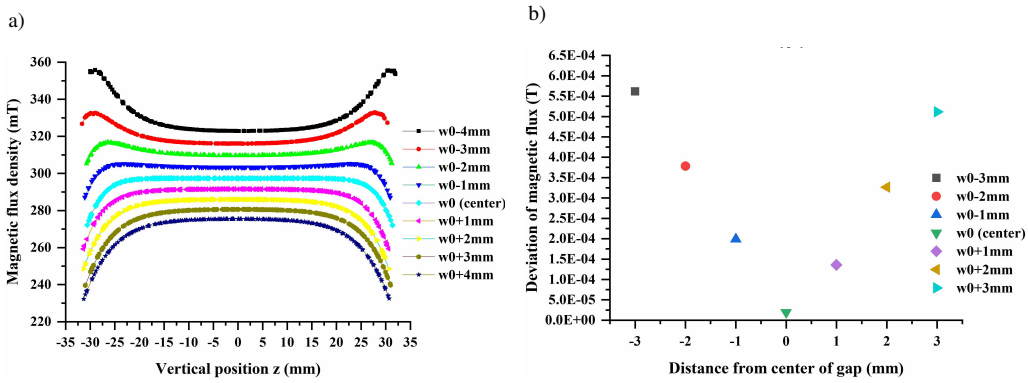

Fig. 8. Horizontal magnetic flux (a) magnetic flux density with different steps of air gap width (b) deviation of magnetic flux at different steps of air gap width.

4.3.2. The effect of air gap width

The magnetic flux was also investigated at different gap widths, while the magnet's height was kept constant. As shown in Fig. 9, the FEA was used to simulate magnetic flux density changes at the air gap center as a function of air gap width at vertical position Z. The magnetic flux variation was studied for different widths: 17, 18, 19, 20, 21, 22, and 23 mm. It can be observed that with a gap width extended by one millimeter, the flux density value drops by around 3%. A gap of 17 mm gives a flat magnetic flux with a small relative deviation.

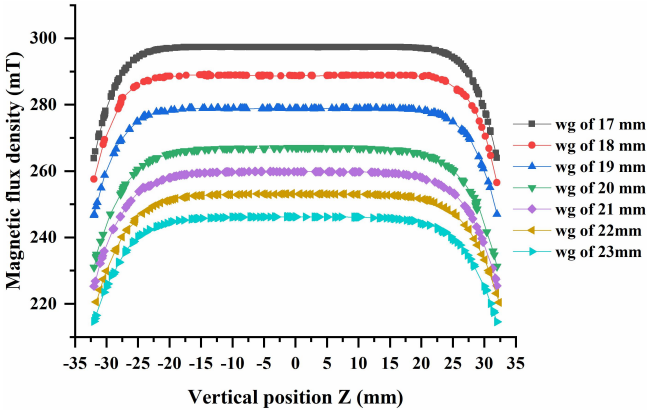

Fig. 9. Magnetic flux density at the vertical position Z for different air gap widths.

4.3.3. Magnetic flux versus relative permeability of yoke material

The yoke is a major element of the magnet system design as it acts as a shield for both the coil and the test mass. To enhance the uniformity of magnetic flux within the air gap, the yoke material must have high permeability, maximum saturation induction, and low hysteresis loss. Soft magnetic materials, such as Ni-Fe alloy, pure iron and low-carbon steel were used for the yoke's manufacturing [18, 20]. FEA was used to study the magnetic flux density in the air gap as a function of relative permeability in order to choose the yoke's manufacturing material, as shown in Figure 10. A significant variation in the value of the magnetic flux can be noticed for materials with a relative permeability of less than 1000. When the relative permeability of the yoke exceeds 1000, the change in the magnetic flux value becomes quite minimal. For NIS's permanent magnet system, low-carbon steel with a relative permeability higher than 2700 was selected as the yoke material.

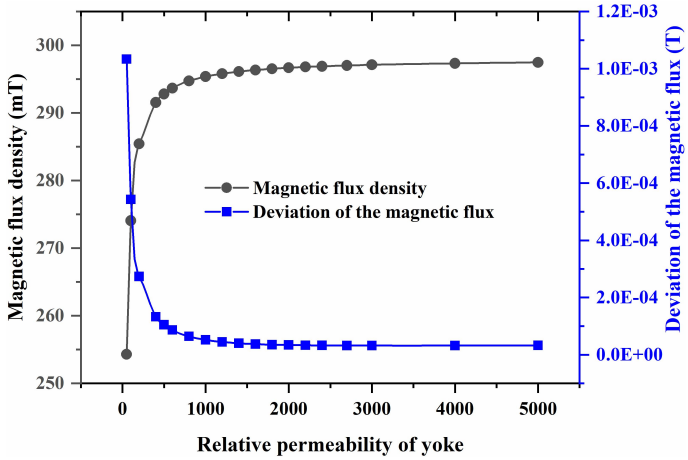

Fig. 10. Magnetic flux density and its deviation with yoke relative permeability.

Metrol. Meas. Syst., Vol. 30 (2023), No. 1, pp. 3–16
DOI: 10.24425/mms.2023.144397

5. Conclusions

In carrying out this study, a prototype of KB employing accessible equipment was designed and developed at the NIS. The magnet system was designed based on a symmetrical permanent magnet system with a yoke. An analytical model and finite element analysis were used to design the magnet system, calculate the magnetic flux value, and optimize the magnetic profile in the air gap. The results showed good agreement between the analytical model and simulation, with a relative difference of 5%. This difference is due to the analytical model, which indicates the flux density value in the gap is produced in the absence of both saturation of the field in the yoke material and flux leakage. The magnetic field uniformity in the air gap was checked using the FEA. The magnetic field uniformity stayed within a range of 8×10^{-5} in the center over a vertical distance of ±15 mm. The FEA was used to investigate and optimize several aspects that influence the magnetic profile, such as air gap width, and yoke material. With a gap width of 17 mm, magnetic flatness is optimal with a slight relative deviation. As well, the magnetic flux density variation in the air gap may be decreased to a few parts in 10^5 by using a low-carbon steel material or different alloys with high relative permeability. These studies and improvements outlined above for the magnet system would enhance the performance of the Kibble balance and reduce target uncertainty.

Appendices

A. Convergence of simulation results

The most common parameter affecting the simulation results is an inadequate mesh. It is necessary to verify and enhance the quality of the mesh since it is one of the most crucial elements that must be taken into account to ensure simulation accuracy. In this study, we have focused on checking the shape of the corner at the air gap end and the effect of the total number of mesh elements. Special consideration was given to the design of the corner at the air gap's end. The simulation outcomes were observed to have been improved by rounding the sharp corners at the air gap end rather than the sharp corner. Additionally, the simulation was run with several user-defined mesh configurations to choose the best mesh. Figure A.1 shows the total mesh elements

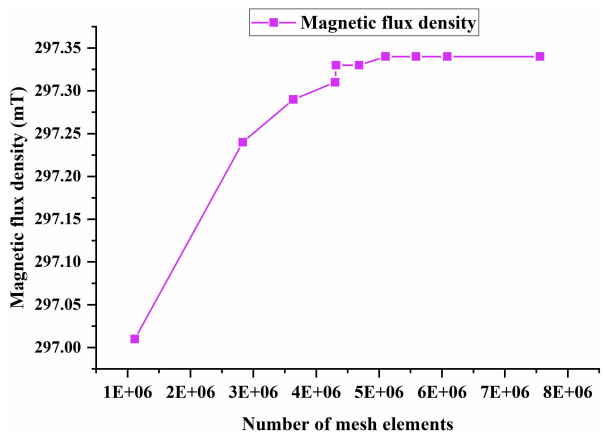

Fig. A.1. Total number of mesh elements as a function of magnetic flux density.

as a function of the magnetic flux value at the air gap's center. The results show a steady value of magnetic flux density with a total number of mesh elements greater than 5×10^6. So, we can assume that the 7,558,093 mesh elements are enough to provide higher-quality mesh elements and the best possible shape of the magnetic field in the air gap.

To achieve higher element quality, a precise choice of mesh parameters (element size parameters) in different user-controlled mesh was carried out, as shown in Fig. A.2.

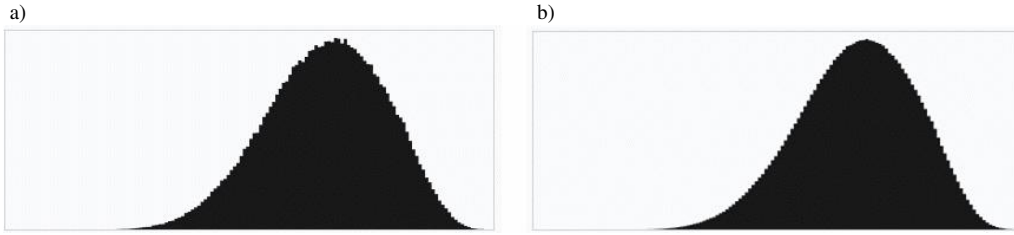

Fig. A.2. Histogram of element quality (a) with the number of mesh elements 1115336 (b) with the number of mesh elements 7558093.

Furthermore, the mesh plot is a useful tool to inspect the quality of mesh elements. A mesh plot can explain the worst qualities of elements and where they are located. Figure A.3 shows the maximum and minimum element quality displayed at the color bar for the air gap domain with different quality mesh elements.

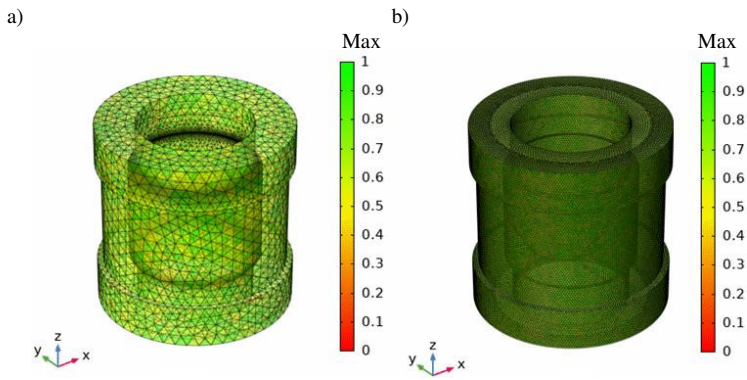

Fig. A.3. Elements quality of air gap domain (a) elements with low quality (b) elements with high quality.

References

[1] Schlamminger, S., & Bettin, H. (2016). Realization, Maintenance and Dissemination of the Kilogram in the Revised SI. *Metrologia*, *53*(5), A1–A5. https://doi.org/10.1088/0026-1394/53/5/A1

[2] International Bureau of Weights and Measures. (2018). Resolution Adopted at the 26th CGPM Meeting.

[3] Wood, B., & Bettin, H. (2019). The Planck constant for the definition and realization of the kilogram. *Annalen der Physik*, *531*(5), 1800308. https://doi.org/10.1002/andp.201800308

[4] Milton, M. J., Davis, R., & Fletcher, N. (2014). Towards a new SI: a review of progress made since 2011. *Metrologia*, *51*(3), R21. https://doi.org/10.1088/0026-1394/51/3/R21

Metrol. Meas. Syst., Vol. 30 (2023), No. 1, pp. 3–16
DOI: 10.24425/mms.2023.144397

[5] Li, S. S., Zhang, Z. H., Zhao, W., Li, Z. K., & Huang, S. L. (2014). Progress on accurate measurement of the Planck constant: Watt balance and counting atoms. *Chinese Physics B*, *24*(1), 010601. https://doi.org/10.1088/1674-1056/24/1/010601

[6] Steiner, R. (2012). History and progress on accurate measurements of the Planck constant. *Reports on Progress in Physics*, *76*(1), 016101. https://doi.org/10.1088/0034-4885/76/1/016101

[7] Fujii, K., Bettin, H., Becker, P., Massa, E., Rienitz, O., Pramann, A., Nicolaus, A., Kuramoto, N., Busch, I., & Borys, M. (2016). Realization of the kilogram by the XRCD method. *Metrologia*, *53*(5), A19. https://doi.org/10.1088/0026-1394/53/5/A19

[8] Robinson, I. A., & Schlamminger, S. (2016). The watt or Kibble balance: a technique for implementing the new SI definition of the unit of mass. *Metrologia*, *53*(5), A46. https://doi.org/10.1088/0026-1394/53/5/A46

[9] Haddad, D., Seifert, F., Chao, L. S., Li, S., Newell, D. B., Pratt, J. R., Williams, C., & Schlamminger, S. (2016). Invited Article: A precise instrument to determine the Planck constant, and the future kilogram. *Review of Scientific Instruments*, *87*(6), 061301. https://doi.org/10.1063/1.4953825

[10] Weights of classes E1, E2, F1, F2, M1, M2, M3, Committee Draft OIML/CD R 111-1 of Edition 2004

[11] Schlamminger, S., & Haddad, D. (2019). The Kibble balance and the kilogram. *Comptes Rendus Physique*, *20*(1–2), 55–63. https://doi.org/10.1016/j.crhy.2018.11.006

[12] Stock, M. (2012). Watt balance experiments for the determination of the Planck constant and the redefinition of the kilogram. *Metrologia*, *50*(1), R1. https://doi.org/10.1088/0026-1394/50/1/R1

[13] Li, S., Stock, M., & Schlamminger, S. (2018). A new magnet design for future Kibble balances. *Metrologia*, 55(3), 319–325. https://doi.org/10.1088/1681-7575/aab2ea

[14] Bielsa, F., Lu, Y. F., Lavergne, T., Kiss, A., Fang, H., & Stock, M. (2015). Alignment of the magnetic circuit of the BIPM watt balance. *Metrologia*, *52*(6), 775–782. https://doi.org/10.1088/0026-1394/52/6/775

[15] Seifert, F., Panna, A., Li, S., Han, B., Chao, L., Cao, A., Haddad, D., Choi, H., Haley, L., & Schlamminger, S. (2014). Construction, measurement, shimming, and performance of the NIST-4 magnet system. *IEEE Transactions on Instrumentation and Measurement*, *63*(12), 3027–3038. https://doi.org/10.1109/TIM.2014.2323138

[16] Baumann, H., Eichenberger, A., Cosandier, F., Jeckelmann, B., Clavel, R., Reber, D., & Tommasini, D. (2013). Design of the new METAS watt balance experiment Mark II. *Metrologia*, *50*(3), 235. https://doi.org/10.1088/0026-1394/50/3/235

[17] Kim, D., Woo, B. C., Lee, K. C., Choi, K. B., Kim, J. A., Kim, J. W., & Kim, J. (2014). Design of the KRISS watt balance. *Metrologia*, *51*(2), S96. https://doi.org/10.1088/0026-1394/51/2/S96

[18] Li, S., Bielsa, F., Stock, M., Kiss, A., & Fang, H. (2017). A permanent magnet system for Kibble balances. *Metrologia*, *54*(5), 775. https://doi.org/10.1088/1681-7575/aa71db

[19] Schlamminger, S. (2012). Design of the permanent-magnet system for NIST-4. *IEEE Transactions on Instrumentation and Measurement*, *62*(6), 1524–1530. https://doi.org/10.1109/TIM.2012.2230771

[20] Solecki, M., Szumiata, T., & Rucki, M. (2021). A novel automatic mass comparator with a resolution of 10 ng for calibration of masses below 2 mg. *Precision Engineering*, *72*, 576–582. https://doi.org/10.1016/j.precisioneng.2021.07.006

[21] Tommasini, D., Baumann, H., Eichenberger, A., & Vorotszhov, A. (2016). The ultra-stable magnet of the Mark II experiment. *IEEE Transactions on Applied Superconductivity*, *26*(4), 1–5. https://doi.org/10.1109/TASC.2016.2521432

[22] Li, S., Zhang, Z., & Han, B. (2013). Nonlinear magnetic error evaluation of a two-mode watt balance experiment. *Metrologia*, *50*(5), 482. https://doi.org/10.1088/0026-1394/50/5/482

[23] Marangoni, R. R., Haddad, D., Seifert, F., Chao, L. S., Newell, D. B., & Schlamminger, S. (2019). Magnet system for the quantum electromechanical metrology suite. *IEEE Transactions on Instrumentation and Measurement*, *69*(8), 5736–5744. https://doi.org/10.1109/TIM.2019.2959852

[24] Li, S., Schlamminger, S., & Wang, Q. (2020). A simple improvement for permanent magnet systems for Kibble balances: More flat field at almost no cost. *IEEE Transactions on Instrumentation and Measurement*, *69*(10), 7752–7760. https://doi.org/10.1109/TIM.2020.2981983

[25] Li, S., & Schlamminger, S. (2022). The irony of the magnet system for Kibble balances – a Review. *Metrologia*, *59*(2), 022001. https://doi.org/10.1088/1681-7575/ac464a

[26] Li, S., Zhao, W., & Huang, S. (2016). A discussion of Bl conservation on a two dimensional magnetic field plane in watt balances. *Measurement Science and Technology*, *27*(5), 051001. https://doi.org/10.1088/0957-0233/27/5/051001

Sayed Emira received the M.Sc. degree in solid state physics from the Faculty of Science, Al Azhar University, in 2019. He is currently an assistant researcher in Mass, Density and Pressure Metrology Department of the National Institute of Standards (NIS), Egypt.

E. R. Shaaban received his Ph.D. degree in materials science from the Department of Physics of the Faculty of Science, University of Eotvos Lorand (Hungary) in 2004. He is a Professor of experimental solid state physics and materials science. He is currently Head of the Department Physics, Al-Azhar University, Assiut, Egypt.

Mohamed M. Rashad received the Ph.D. in inorganic chemistry from Ain Shams University in 2002. He has been awarded 5 state prizes in advanced materials technology as well as environmental studies. He is currently Professor Dean of the Institute of Advanced Materials at the Central Metallurgical Research and Development Institute (CMRDI), Egypt.

Shaker A. Gelany received the Ph.D. degree in mechanical design and production engineering from the Faculty of Engineering, University of Cairo, in 2019. He is currently a researcher in Mass, Density and Pressure Metrology Department of the National Institute of Standards (NIS), Egypt.